NASA Technical Memorandum 113160
AIAA–97–3260

Porous and Microporous Honeycomb Composites as Potential Boundary-Layer Bleed Materials

D.O. Davis and B.P. Willis
Lewis Research Center
Cleveland, Ohio

M. Schoenenberger
Case Western Reserve University
Cleveland, Ohio

Prepared for the
33rd Joint Propulsion Conference and Exhibit
cosponsored by AIAA, ASME, SAE, and ASEE
Seattle, Washington, July–6–9, 1997

National Aeronautics and
Space Administration

POROUS AND MICROPOROUS HONEYCOMB COMPOSITES AS POTENTIAL BOUNDARY-LAYER BLEED MATERIALS

D. O. Davis* and B. P. Willis†
NASA Lewis Research Center, Cleveland, Ohio

M. Schoenenberger‡
Case Western Reserve University, Cleveland, Ohio

Abstract

Results of an experimental investigation are presented in which the use of porous and microporous honeycomb composite materials is evaluated as an alternate to perforated solid plates for boundary-layer bleed in supersonic aircraft inlets. The terms "porous" and "microporous," respectively, refer to bleed orifice diameters roughly equal to and much less than the displacement thickness of the approach boundary-layer. A baseline porous solid plate, two porous honeycomb, and three microporous honeycomb configurations are evaluated. The performance of the plates is characterized by the flow coefficient and relative change in boundary-layer profile parameters across the bleed region. The tests were conducted at Mach numbers of 1.27 and 1.98. The results show that the porous honeycomb is not as efficient at removing mass compared to the baseline. The microporous plates were about equal to the baseline with one plate demonstrating a significantly higher efficiency. The microporous plates produced significantly fuller boundary-layer profiles downstream of the bleed region for a given mass flow removal rate than either the baseline or the porous honeycomb plates.

Nomenclature

A_{total}	=	total bleed area
D	=	bleed hole diameter
H_i	=	incompressible shape factor
L	=	bleed hole length
L_{HC}	=	honeycomb cell length
$\dot{m}$	=	mass-flow rate
$\overline{m}$	=	normalized mass-flow rate (eq. 5)
$\dot{m}'_{bl}$	=	unit mass-flow rate in boundary-layer
$\dot{m}^*$	=	ideal choked mass-flow rate (eq. 2)
M	=	Mach number or molecular weight
N	=	number of bleed holes in plate
P_{plen}	=	bleed plenum pressure
P_t	=	total pressure
Q	=	sonic flow coefficient (eq. 1)
Re'	=	unit Reynolds number
S_x	=	axial span of bleed region (Fig. 3)
S_z	=	transverse span of bleed region (Fig. 3)
T_t	=	total temperature
U	=	mean velocity component in x-direction
x,y,z	=	cartesian coordinate system
δ	=	boundary-layer thickness
δ^*	=	displacement thickness
η	=	location of sonic point (y^*/δ)
θ	=	momentum thickness

Subscripts

0	=	condition in wind-tunnel plenum
1	=	condition at Station 1 (Fig. 4)
2	=	condition at Station 2 (Fig. 4)
e	=	boundary layer edge condition
i	=	incompressible

Introduction

WHEN bleed is used as a means to control boundary-layer separation, the performance of the bleed configuration is typically characterized by the efficiency with which it can remove boundary-layer mass and by the improvement in boundary-layer distortion as a function of bleed mass-flow rate. To minimize bleed drag and system component size, bleed configurations are sought that have a high efficiency and provide acceptable boundary-layer distortion with a minimum of mass removal. Flow coefficient[1–3] and boundary-layer distortion[4, 5] studies in the open literature that are applicable to the design of boundary-layer bleed systems for supersonic inlets are generally restricted to the performance of perforated solid plates with orifice dimensions on the order of the displacement thickness of the approach boundary-layer. From a performance and weight standpoint, it is desirable to keep the bleed plate as thin as possible. Under loading, however, thin bleed plate material is prone to flexing, and as a result, longitudinal stiffeners are typically attached to the plenum side of the bleed plate. The

*Research Engineer, Inlet Branch, Senior Member AIAA.

†Research Engineer, Inlet Branch, Member AIAA.

‡Research Assistant, Dept. of Mechanical and Aerospace Engineering, Student Member AIAA.

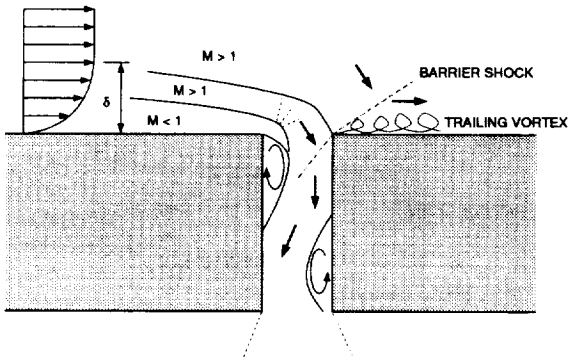

Fig. 1 Flow features in the vicinity of a bleed hole or slot.

stiffeners block bleed orifices, which may have a detrimental effect on overall bleed system performance. At present, there is insufficient data available to accurately assess the performance penalty associated with the stiffeners. A possible alternative that has the potential to meet the required stiffness criteria is to bleed through a perforated composite honeycomb material (backing skin + honeycomb + backing skin). This type of material, which is commonly used in aircraft inlet nacelles, has not been used previously as a bleed material for two reasons: 1) the lack of an aerodynamic database from which to design and 2) the unknown effect of perforations on the structural integrity of the composite. The present investigation is intended to address the former by providing a preliminary aerodynamic evaluation of various honeycomb configurations for possible use as boundary-layer bleed materials.

A schematic illustrating some of the flow features that have been observed in the vicinity of a bleed hole or slot are shown in Fig. 1.[6,7] As the flow approaches the hole, there exists a limiting streamline that separates the flow that enters the hole from that which continues in the downstream direction. The low momentum fluid nearest the wall is drawn into the hole fostering a more robust downstream boundary layer. The higher momentum fluid that does not enter the hole must be turned to again flow parallel to the surface. This turning is accomplished by the segment of the barrier shock that extends into the main flow and the accompanying adverse pressure gradient partly negates the benefits gained by bleeding off the low momentum fluid. For a given approach boundary-layer, bleed porosity, and total bleed mass-flow rate, the strength of the barrier shock will increase as the diameter of the orifice increases, since increasingly higher Mach number flow will be turned towards the hole. Based on this, we can speculate that reducing the size of the bleed orifice diameter while maintaining a given porosity may lead to improved downstream boundary-layer distortion. In past bleed system designs, the bleed orifice diameter was scaled to be about the same as the displacement thickness of the approach boundary layer ($D/\delta^* \approx 1$), which seems to have been based, at least in part, on a reluctance to deviate orifice scaling from that used in the existing flow coefficient database.[8] In this study, two honeycomb configurations are investigated where the orifice diameter is roughly the same as the displacement thickness of the boundary layer. These configurations are referred to as "porous honeycomb composites." In addition, three honeycomb configurations are tested where the orifice diameter is much smaller than the displacement thickness ($D/\delta^* << 1$). These configurations are referred to as "microporous honeycomb composites."

Experimental Program

Bleed Plate Configurations

In all, five different honeycomb configurations and one baseline perforated solid plate were investigated. The geometry of the six bleed configurations are summarized in Table 1. Photographs of the flow side and bleed plenum side of four of the plates are shown in Fig. 2. The span of the bleed region in the x and z–directions (S_x and S_z) given in Table 1 is defined as shown in Fig. 3.

Table 1 Bleed Plate Configurations

Plate	C1	HC1	HC2	MP1	MP2	MP3
D (mm)	6.350	6.350	3.175	0.203	0.368	0.239
L/D	1	0.1	0.2	1	1	1
L_{HC}/D	N/A	1.75	3.5	47	26	40
N	75	87	348	85,000	43,000	173,000
A_{total} (mm^2)	2375.0	2755.0	2755.0	2076.0	4844.0	7150.0
Porosity (%)	19.64	35.06	35.06	9.0	21.0	31.0
S_x (mm)	69.85	50.4	50.4	139.7	139.7	139.7
S_z (mm)	152.4	148.6	148.6	165.1	165.1	165.1

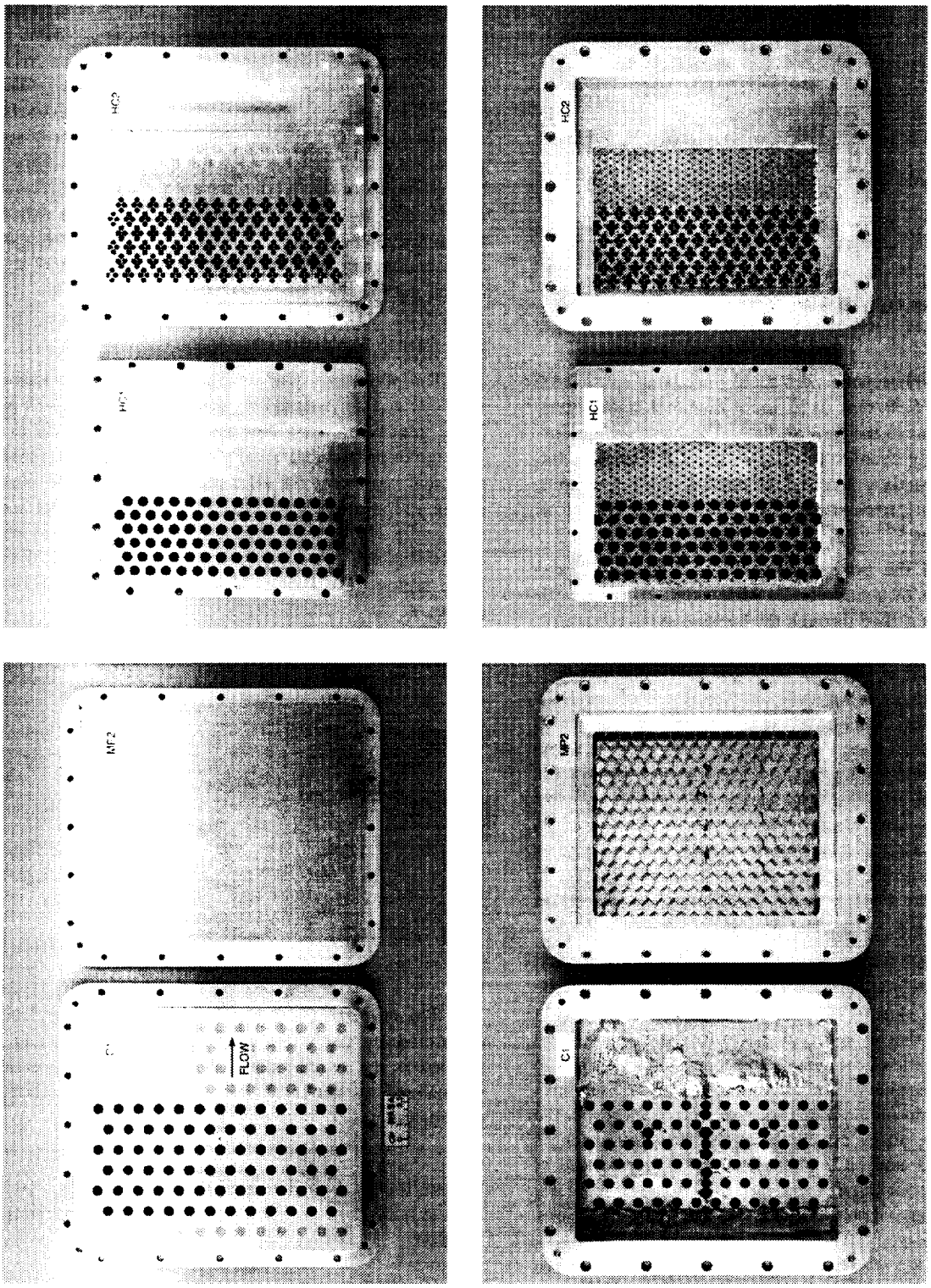

Fig. 2 Photographs of bleed plates (L-R): C1, MP2, HC1, HC2. Top row is flow side, bottom row is plenum side.

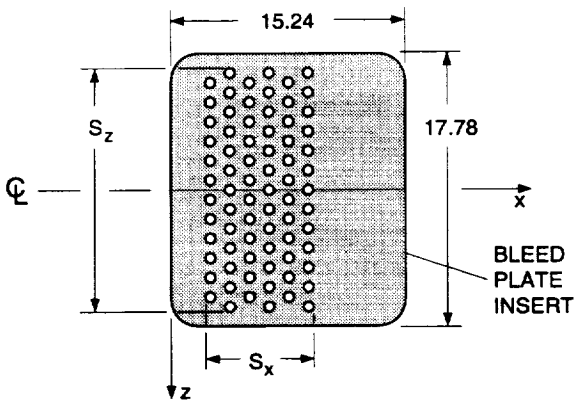

Fig. 3 Plan view of bleed insert (C1 plate shown).

The baseline solid perforated plate, C1, consists of six rows of 6.35 mm (0.25 inch) diameter round holes drilled normal to the flow surface. The bleed hole diameter is roughly equal to the displacement thickness of the approach boundary layer. This plate was a pre-existing plate used in previous boundary layer bleed studies at NASA Lewis.[3-5]

Two of the honeycomb configurations, HC1 and HC2, consist of actual nacelle honeycomb material with hole patterns drilled through the backing skins concentric with the individual cells. The HC1 plate has a single hole per cell, whereas the HC2 plate has four holes per cell. The flow area entering each individual cell of the HC1 and HC2 plates is nominally the same as the hole area in the C1 baseline plate. The spacing of the hole patterns on the HC1 and HC2 plates is closer together than the C1 baseline plate resulting in a significantly higher porosity in the honeycomb plates. The nacelle material used to fabricate the HC1 and HC2 plates already had small holes through one of the backing skins. As shown in Fig. 2, the side of the plate with the small holes was placed on the plenum side of the test article.

The microporous honeycomb plates, MP1, MP2 and MP3, are purely research articles fabricated by gluing the microporous skin to a frame and backing the skin with honeycomb that is spot glued to the skin. A ridge on the plenum side of the plate also supports the honeycomb around its periphery. The microporous plates do not have a backing skin on the bleed plenum side. As a result, the microporous plates do not have the structural strength that the HC1 and HC2 plates have. Another feature of the microporous skins is that the holes in the skin are not straight through holes, but are shaped like converging-diverging nozzles. The exact contour of the orifices is not known, but it is known that the throat of the orifice is biased toward one side of the skin. This feature was not known at the time the skins were mounted and as a result the MP1 and MP3 skins were mounted with the throat biased toward the bleed plenum side of the bleed plate and the MP2 skin was mounted with throat biased toward the flow side of the plate.

The bleed area given in Table 1 for the C1, HC1, and HC2 plates is based on measurement of the hole diameter and the uncertainty of the calculated area is estimated to be less than ±1%. The bleed area given for the MP1, MP2, and MP3 plates are based on the porosity provided by the skin supplier. Measurement of the hole diameter and spacing under a microscope indicated that the actual porosity is slighlty higher than the quoted value. This at least partially offset by the presence of the honeycomb and the backing ridge which partially blocks the exit of the honeycomb cells near the edge of the plate. Based on these condsiderations, the uncertainty in the bleed area for the microporous plates is estimated to be ±4%.

Performance Evaluation

The performance of the six bleed configurations is characterized by two sets of measurements. The first set is the total bleed mass flow through the test article as a function of normalized bleed plenum pressure. This measurement represents the efficiency with which the bleed configuration can remove boundary-layer mass. The second is the characteristics of the boundary layer at reference stations located upstream and downstream of the bleed region. The locations of these stations are shown in Fig. 4.

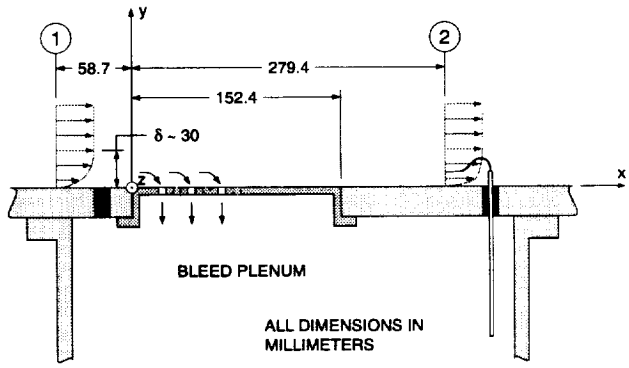

Fig. 4 Bleed region schematic.

The efficiency of a bleed configuration is typically quantified by the sonic flow coefficient, Q, which is defined as the actual mass flow through a bleed region normalized by the ideal mass flow rate under choked conditions:

$$Q = \frac{\dot{m}}{\dot{m}^*} \tag{1}$$

For air, the ideal choked mass flow in standard liters per minute (slm) is determined from the following isentropic relation:

$$\dot{m}^*(\text{slm}) = 2.015 \frac{P_{t,s}(\text{kPa}) A_{total}(\text{mm}^2)}{\sqrt{T_{t,s}(\text{K})}} \tag{2}$$

where A is the cross-sectional area of the bleed orifice(s). For the purposes of data reduction, the boundary-layer

edge total pressure ($P_{t,e}$) and total temperature ($T_{t,e}$) are assumed to be the same as the wind tunnel plenum total pressure ($P_{t,0}$) and total temperature ($T_{t,0}$) , respectively. The sonic flow coefficient is usually presented as a function of the bleed plenum pressure normalized by the freestream total pressure ($P_{plen}/P_{t,e}$). The distortion of the boundary layer is usually quantified by a distortion parameter such as the incompressible shape factor:

$$H_i = \frac{\delta_i^*}{\theta_i} = \frac{\int_0^\delta \left(1 - \frac{U}{U_e}\right) dy}{\int_0^\delta \frac{U}{U_e}\left(1 - \frac{U}{U_e}\right) dy} \tag{3}$$

A fully turbulent, zero pressure gradient boundary layer typically has an incompressible shape factor of H_i = 1.29.

Facility and Instrumentation

The experiments were conducted in NASA Lewis' 1×1 ft. Supersonic Wind Tunnel (SWT), which is a continuous flow facility with interchangeable fixed geometry Laval nozzles. A schematic of the 1×1 ft. SWT is shown in Fig. 5. The approach boundary layer is the naturally occurring boundary layer on the wind-tunnel wall and is bled through the honeycomb test article into a large bleed plenum. The bleed mass-flow rate is controlled by a translatable mass-flow plug and bleed vacuum is supplied by lab-wide altitude exhaust and a 450 psi air ejector system.

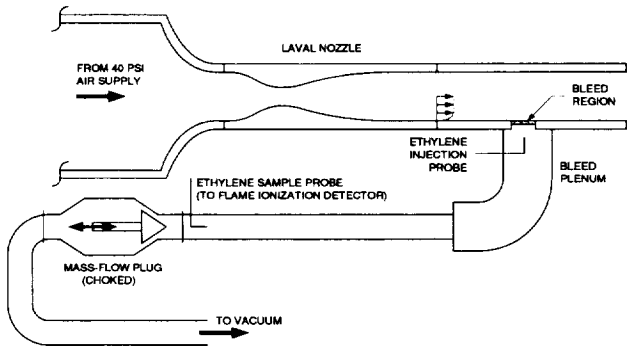

Fig. 5 Wind tunnel schematic.

The experiment was instrumented to measure wind tunnel plenum total pressure and temperature, total mass-flow through the bleed plates, nozzle and test section surface static pressure, bleed plenum pressure, and boundary-layer Pitot pressure.

The total bleed mass flow was measured using the ethylene trace gas method-of-mixtures technique described by Davis *et al.*[9] With reference to Fig. 5, pure ethylene is injected at a known mass-flow rate into the bleed plenum with a forward facing probe. The ethylene mixes thoroughly with the bleed flow and then a sample of the mixture is extracted just upstream of the mass-flow plug. The concentration of the ethylene in the sample is measured and the bleed mass-flow rate is then calculated from the following relation:

$$\dot{m}_{air} = \left(\frac{M_{air}}{M_{eth}}\right)\left(\frac{1 - v_{eth}}{v_{eth}}\right)\dot{m}_{eth} \tag{4}$$

where M_{air} and M_{eth} are the molecular weight of air and ethylene, respectively, $\dot{m}_{eth}$ is the injection mass flow rate of ethylene, and v_{eth} is the volume fraction of ethylene after thorough mixing. The ethylene flow rate was controlled by an Edwards Model 825 Mass Flow Controller. The uncertainty of the Edwards ethylene mass flow controller is taken to be the manufacturers quoted uncertainty of ±1.0%. The volume fraction was measured with a Gow-Mac Model 23–500 Flame Ionization Detector. The uncertainty of this measurement is based on experience and is estimated to be ±2%.

The boundary-layer profiles were measured with a round 0.381 mm diameter Pitot tube probe with square leading edge and having an inner-to-outer diameter ratio of 0.4. The probe pressure was measured with Pressure Systems Incorporated Electronically Scanned Pressure (ESP) 0–15 psia (±103 kPa) range pressure transducer. Surface static pressure data were measured with conventional 0.508 mm diameter static pressure taps. The tap data were measured with ESP ±5 psid (±34.5 kPa) range pressure transducers.

The pressure measurement and temperature measurement uncertainty was estimated using Blumenthal's PC program.[10] The pressure measurements are estimated to have an overall uncertainty of ±0.15% and the wind tunnel total temperature is estimated to have an uncertainty of ±2.5%.

Results and Discussion

Reference Boundary-Layer Profiles at Stations 1 and 2

Reference boundary-layer profiles were measured in the plane of symmetry at data stations (DS) 1 and 2 (see Fig. 4) for freestream Mach numbers of 1.27 and 1.98. The reference profile at DS2 was obtained with a blank plate installed in place of a bleed plate. The characteristics of these boundary layers are summarized in Table 2. The Mach number distribution in the boundary layer was computed from the Pitot pressure and the local wall static pressure (static pressure was assumed constant across the boundary-layer) using the Rayleigh-Pitot formula. The velocity distribution was then obtained from the Mach number and an assumed temperature distribution based on the adiabatic Crocco relation with the recovery factor specified as 0.89. The probe-wall touch was established by electrical continuity.

Table 2 Reference boundary-layer parameters.

M	1.27		1.98	
	DS1	DS2	DS1	DS2
$P_{t,0}$ kPa	89.7	89.7	137.7	137.7
$T_{t,0}$ K	287	290	283	284
$Re' \times 10^7$ /m	1.42	1.41	1.85	1.85
δ mm	24.8	27.9	23.8	26.6
δ^* mm	4.23	4.96	5.28	6.03
θ mm	2.20	2.58	1.87	2.15
H_i	1.29	1.30	1.28	1.29
η %	29.1	34.3	1.85	2.75
$\dot{m}'_{bl}$ kg/s/m	4.15	4.56	3.76	3.98

Sonic Flow Coefficient

The sonic flow coefficient was calculated for each plate from eqs. 1, 2, and 4. Using the individual measurand uncertainties given in previous sections, the propagation of uncertainty into the sonic flow coefficient yields a sonic flow coefficient uncertainty interval of ±2.75% for the C1, HC1, and HC2 plates. For the MP1, MP2, and MP3 plates the sonic flow coefficient uncertainty interval is ±4.75%. The increase in uncertainty for the microporous plates is due to the higher uncertainty in the total bleed area.

Sonic flow coefficient distributions for the C1 baseline plate are shown in Fig. 6 for both operating conditions summarized in Table 2. In this plot, the current data measured using the method-of-mixtures are compared to previous data taken several years ago using an ASME venturi. As a check of repeatability, the method-of-mixture surveys were performed twice. For the M=1.27 case, the agreement of the present results with the old venturi results is very good. For the M=1.98 case, the method of mixture distributions lie slightly higher than the ASME venturi distribution. The reason for the difference is not known but may be related to the ASME venturi being operated at a Reynolds number below its calibration range. Since all the flow coefficient data for the present study were obtained using the method-of-mixtures, all comparisons to the baseline case, C1, will be to the method-of-mixture distributions shown in Fig. 6.

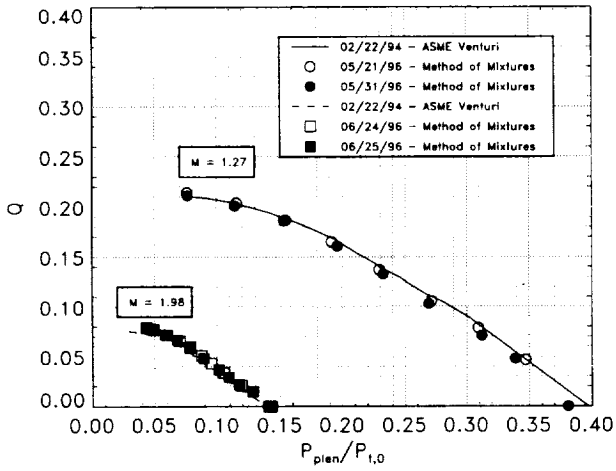

Fig. 6 Flow coefficient curve for C1 baseline plate.

Sonic flow coefficient distributions for the porous honeycomb configurations HC1 and HC2 are shown in Fig. 7a and Fig. 7b, respectively. Due to time constraints, data were obtained only at M=1.27 for these cases. The solid line distribution shown in these plots is the baseline C1 case. For the HC1 plate (single hole per cell), the dis-

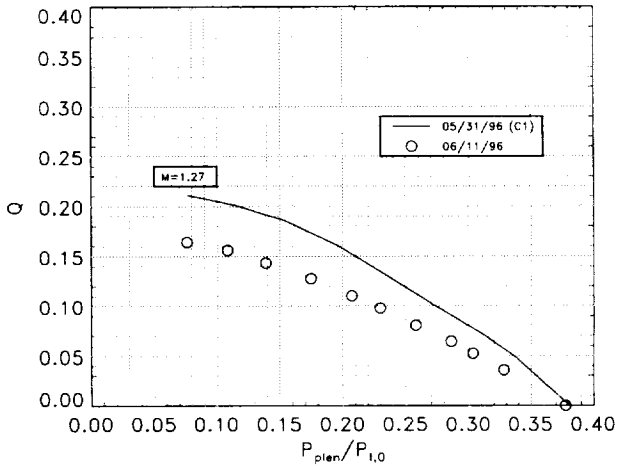

a) HC1 plate.

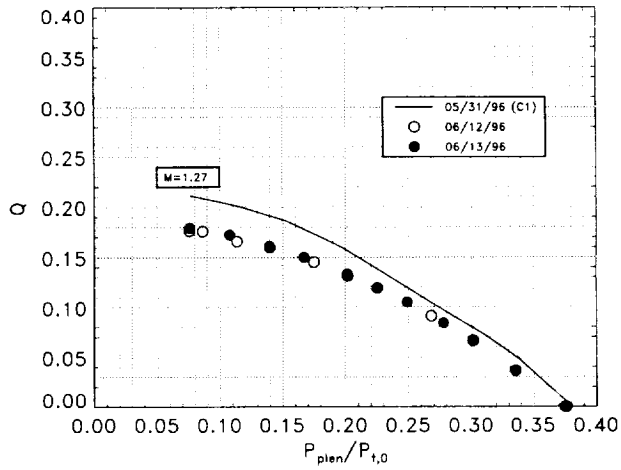

b) HC2 plate.

Fig. 7 Flow coefficient curves for HC1 and HC2 honeycomb plates.

tribution lies consistently about 21 percent lower than the baseline case. For the HC2 plate (four holes per cell), the situation improves slightly, but still the distribution lies about 14 percent lower than the baseline case. Also note that the surveys for the HC2 case were performed twice. The degradation in performance over the baseline case is not surprising since with the honeycomb, the bleed flow first expands into the honeycomb cell, but then must contract to exit through the plenum side backing skin hole. This expansion and contraction through the square-edged orifices can account for the additional losses. Another cause may be related to the higher porosity of the honeycomb plates, whereby interaction between the jets exiting into the bleed plenum inhibits full expansion of the flow.

There are two possible explanations for the improvement in performance of the HC2 plate over the HC1 plate. First, the four holes per cell configuration of the HC2 plate results in more streamwise hole edges than the HC1 plate which is speculated to promote turning of the flow into the hole.[3] Second, the material between the four holes acts as a compression surface which leads to higher local pressure over the downstream hole in the four-hole pattern of each cell. Davis *et al.*[11] have shown that two normal bleed holes spaced two diameters apart will flow 4.5% higher mass flow at M=1.62 when positioned in line with the flow direction when compared to being positioned normal to the flow direction. At M=2.49, the increase in flow rate is roughly 6.0%.

Sonic flow coefficient distributions for the microporous honeycomb configurations MP1, MP2, and MP3 are shown in Fig. 8a, Fig. 8b, and Fig. 8c, respectively. For these plates both M=1.27 and M=1.98 cases are considered. With reference to Fig. 8a, the MP1 plate distributions lie approximately *75% higher* than the baseline distributions. This behavior is somewhat surprising considering that the MP2 and MP3 microporous plate distributions are quantitatively similar to the baseline plate, i.e., they behave like "regular" normal holes. To ensure that nothing had gone amiss in the data accumulation and reduction, the survey for the M=1.27 case was repeated three times with surveys of the baseline case performed between repeats with the same results. We next considered that the porosity of the skin was actually much higher than what was quoted by the supplier. However, as mentioned earlier, microscopic inspection of the skin indicated that the porosity was nominally the same as the supplier quoted. The reason for the MP1 plate behavior is not clear at this point and further testing and inspection is planned to understand what is happening with this particular configuration.

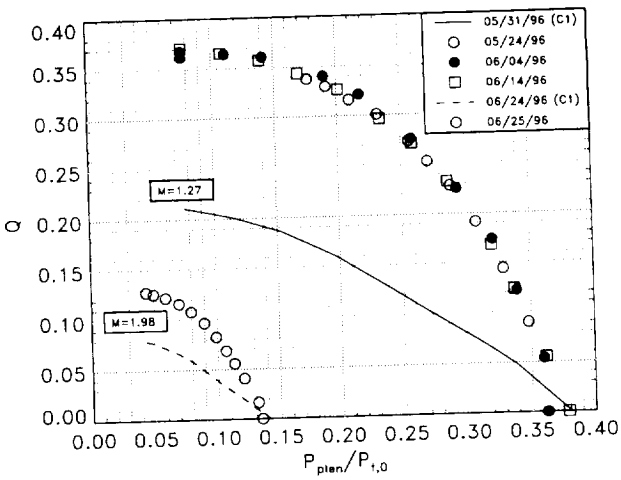

a) MP1 plate (9% porosity).

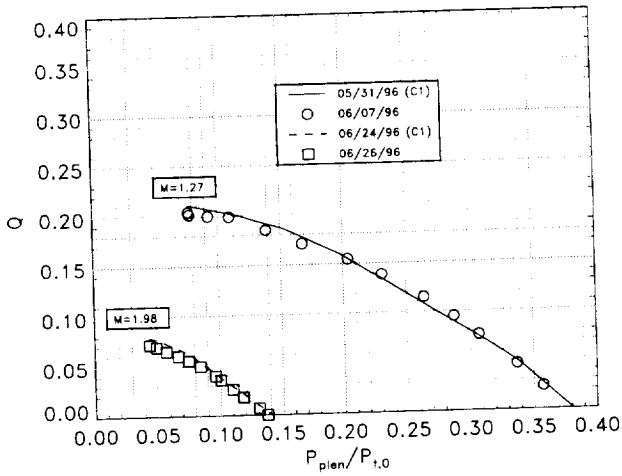

b) MP2 plate (21% porosity).

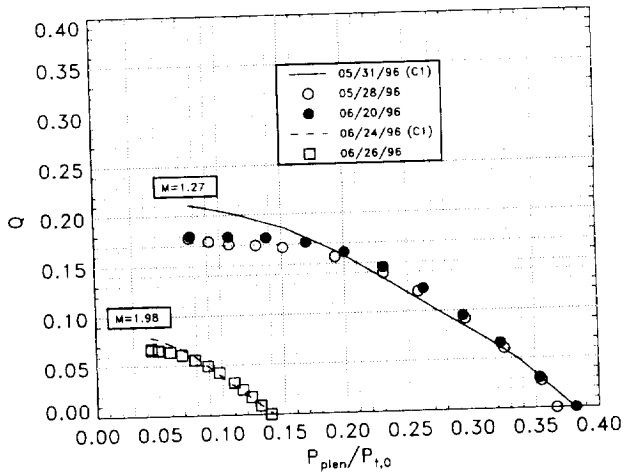

c) MP3 plate (31% porosity).

Fig. 8 Flow coefficient curves for MP1, MP2 and MP3 microporous plates.

The flow coefficient distributions for the MP2 plate (Fig. 8b) are about the same as the C1 baseline case up until the near-choked bleed rate, at which point the MP2 curve appears to flatten out slightly. This behavior is observed at both Mach numbers, although slightly more pronounced for the M=1.98 case. This slight deviation, however, is on the order of the precision (random) uncertainty in the measurements and may or may not be significant.

The flow coefficient distributions for the MP3 plate (Fig. 8c) are about the same as the C1 baseline case up until about 3/4 maximum baseline bleed rate, at which point the MP3 curve flattens out significantly. This behavior supports the results of the MP2 plate and suggests that jet interaction in the bleed plenum at the lower pressure ratios inhibits a further increase in flow as the bleed plenum pressure is decreased. Based on the present limited data, the jet interaction effect appears to occur for porosity greater than 20%.

Boundary-Layer Profiles at Station 2 with Bleed

Boundary-layer surveys were performed for each bleed configuration at five roughly equally spaced bleed rates ranging from zero to near choked conditions, i.e., $\dot{m}$ = 0, $0.25Q_{max}$, $0.5Q_{max}$, $0.75Q_{max}$, Q_{max}. The boundary layer profiles plotted in terms of a normalized velocity (U/U_e) are shown for the M=1.27 and 1.98 cases in Figs. 9 and 10, respectively. For the M=1.98 case, surveys for the HC1 and HC2 porous honeycomb plates were not obtained due to time constraints. The solid line profile shown in all of the plots is the reference profile measured at DS 2 with the blank plate installed. The parameters associated with these reference profiles are given in Table 2.

The bleed mass-flow rate for each of the surveys is expressed in terms of a percent of the boundary-layer mass flow at DS 1:

$$\overline{m} = \frac{\dot{m}}{(S_s) \cdot \left(\dot{m}'_{bl,1}\right)} \qquad (5)$$

where S_s is the transverse span of the bleed region given in Table 1. Note that due to the different flow coefficient behavior and total bleed area, this normalized mass flow rate is not the same from configuration to configuration. Also tabulated for each survey is the boundary-layer thickness (δ), the displacement thickness (δ^*), the momentum thickness (θ), the incompressible shape factor (H_i), and the location of the sonic point in the boundary layer ($\eta = y^*/\delta$).

Boundary-layer surveys conducted with the bleed plates installed but with no net bleed flow (profile to the far left of each plot) give an indication of the roughness of the material. The boundary layer thickness and the incompressible shape factor for these profiles increase to some degree over the blank plate reference values (see Table 2) for all of the plate configurations. This roughness effect can be considered to be real for the C1, HC1 and HC2 plates since these plates are quite rigid. For the microporous plates (MP1, MP2, and MP3), the roughness effects are probably less than indicated since the skins were observed to form small waves under no-bleed conditions. This is likely due to the contraction of the frame when installed into the cool wind-tunnel walls and the spot gluing of the skin to the honeycomb. As soon as even the smallest bleed was applied, however, the skins flattened out onto the honeycomb.

For the profiles taken when the bleed flow is non-zero, an increase in bleed flow produces a decrease in all other parameters. A general observation that can be clearly seen is that the microporous plates produce more full velocity profiles near the wall than the porous plates. To quantify this behavior, we can look at a cross-plot of the incompressible shape factor versus the normalized bleed mass-flow rate. These results are shown for the M=1.27 and 1.98 cases in Figs. 11 and 12, respectively. For both Mach numbers, the plots show that the microporous plates (MP1, MP2, and MP3) are more effective at reducing the incompressible shape factor than the porous plates (C1, HC1, and HC2). In fact, the porous plate configurations do not reduce the shape factor much below the reference blank plate value at DS 2. We believe this is due to the local barrier shock located at the trailing edge of each hole. The microporous plates show a reduction in shape factor until about 20 to 25% boundary layer bleed at which point the limited data indicates a rise. This is probably due to a global compression at the end of the bleed plate at high bleed rates.

To illustrate the velocity profile improvement of the microporous skin over the baseline configuration, near wall velocity profiles corresponding to the filled symbols in Fig. 11 and 12 are shown in Fig.13. These cases correspond to the C1 baseline configuration at near-choked bleed and the MP2 microporous skin case at half choked bleed conditions. These cases were chosen for comparison because the normalized bleed mass flow rate and the bleed region porosity are similar. The results show that the MP2 plate produces a significantly fuller profile near the wall. Note that the normalized mass flow for the MP2 plate is actually less than the C1 baseline case for both Mach numbers. Beyond y=1.25 cm (approximately $\frac{1}{2}\delta$) there is little difference in the profiles.

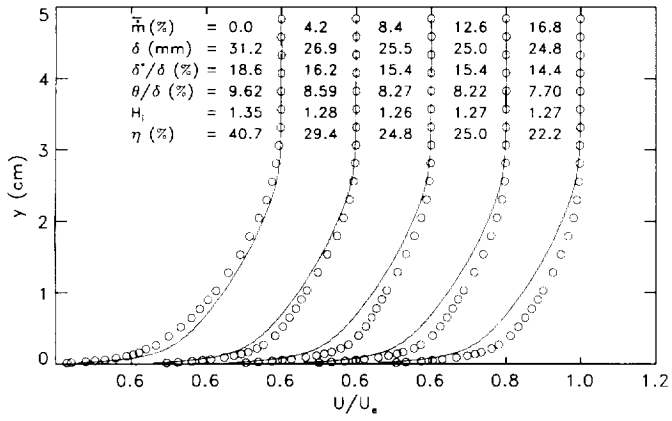

a) C1.

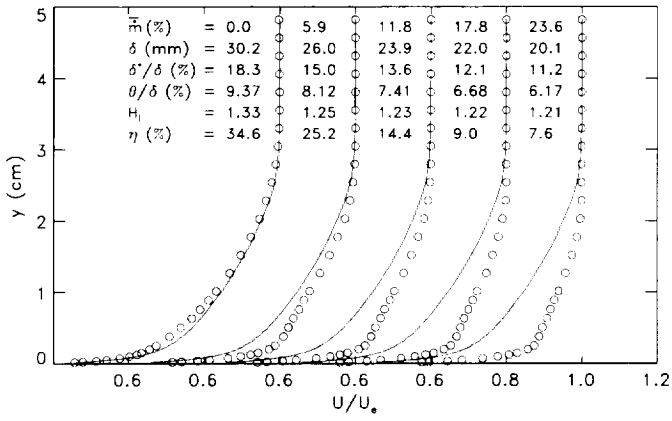

d) MP1.

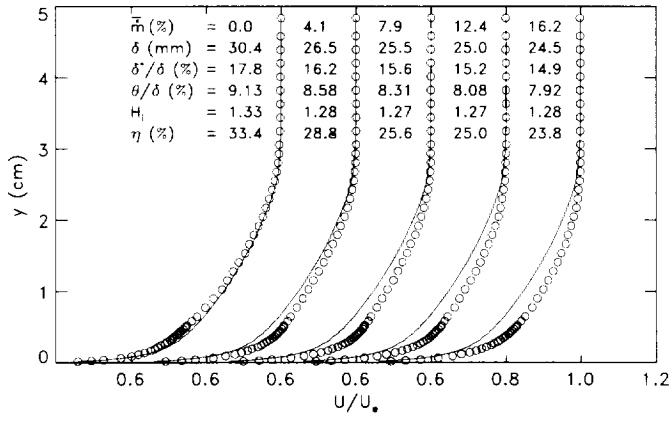

b) HC1.

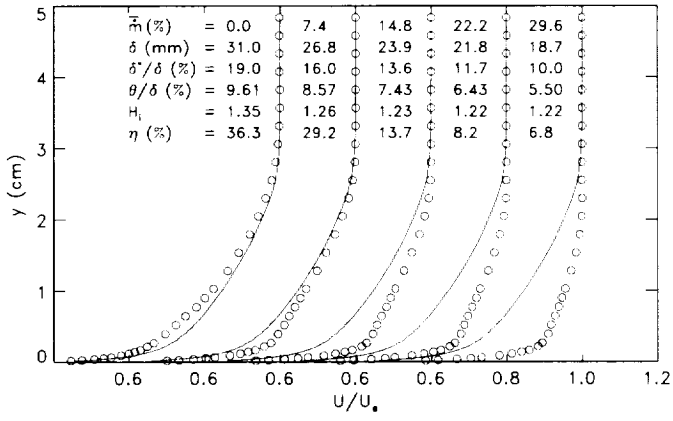

e) MP2.

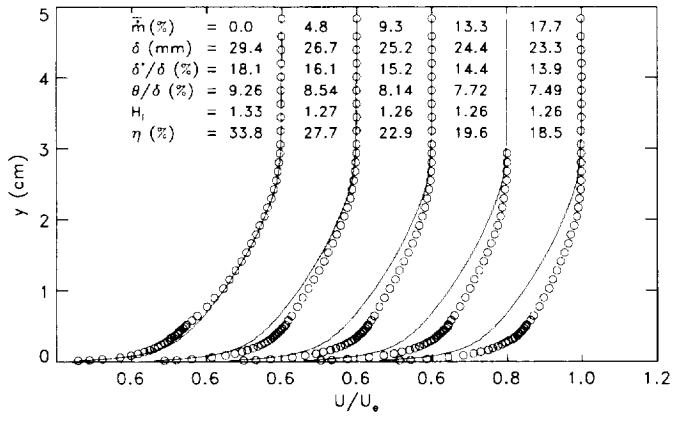

c) HC2.

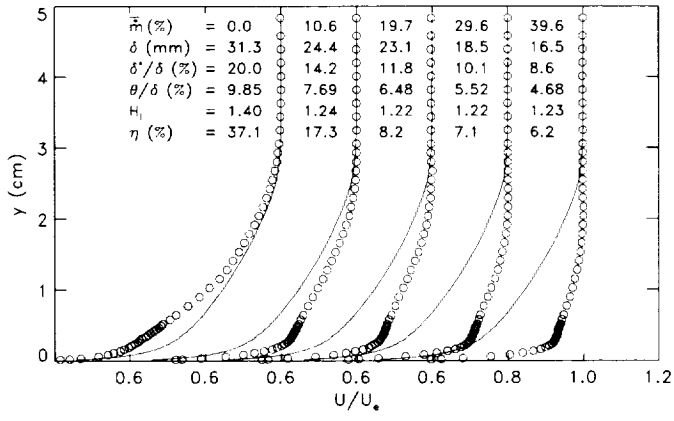

f) MP3.

Fig. 9 Normalized velocity profiles at DS 2, M=1.27.

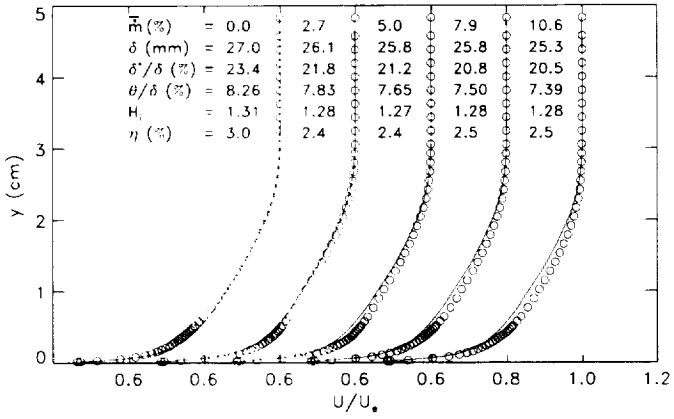

a) C1.

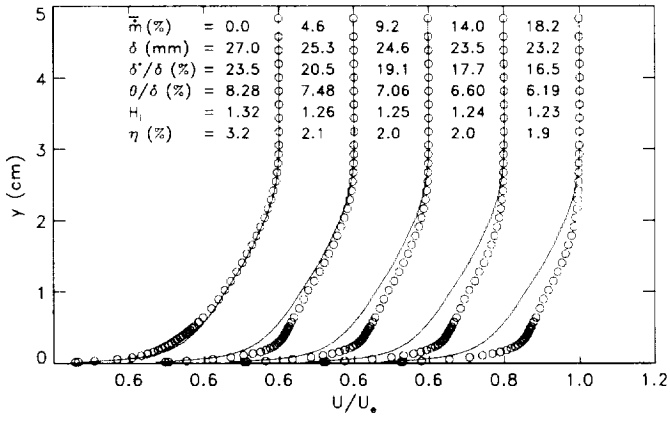

c) MP2.

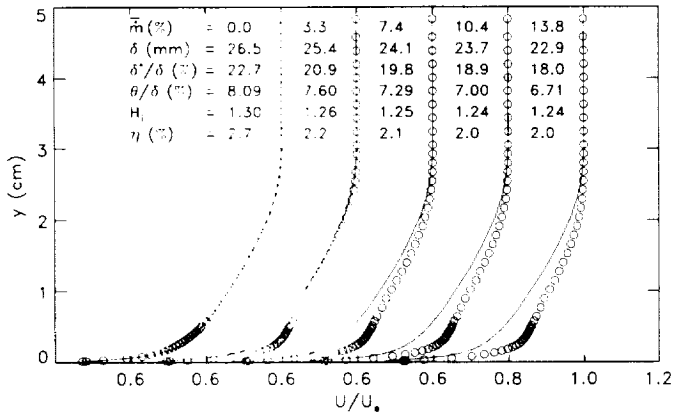

b) MP1.

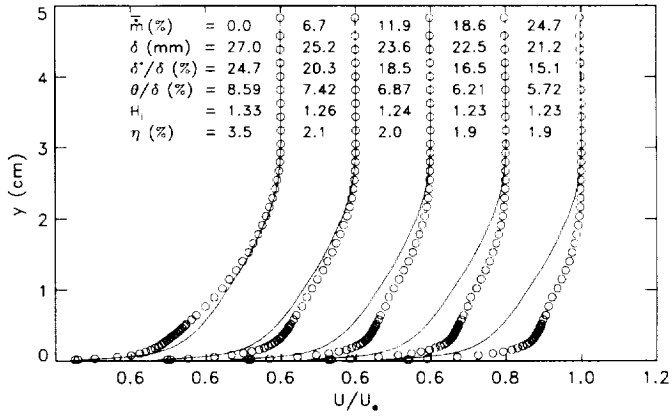

d) MP3.

Fig. 10 Normalized velocity profiles at DS 2, M=1.98.

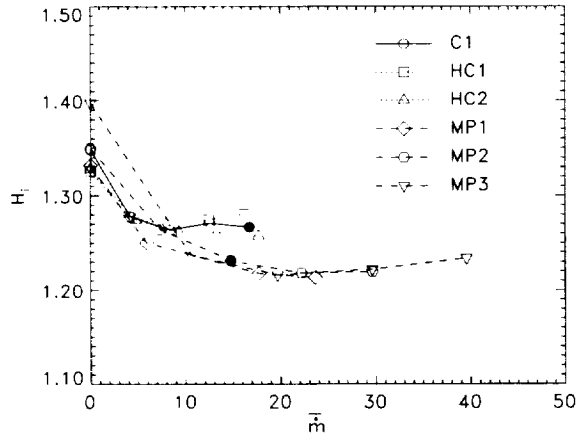

Fig. 11 H_i vs. bleed mass flow, M=1.27.

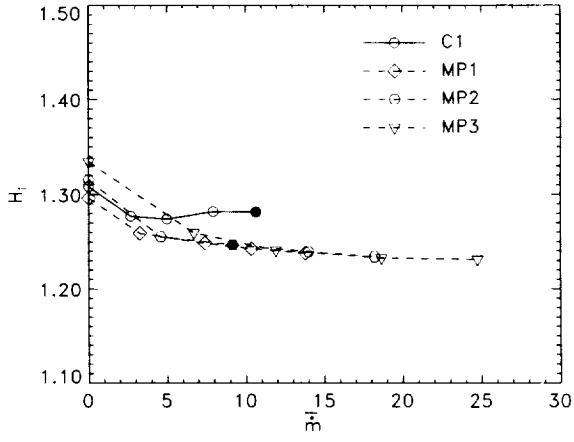

Fig. 12 H_i vs. bleed mass flow, M=1.98.

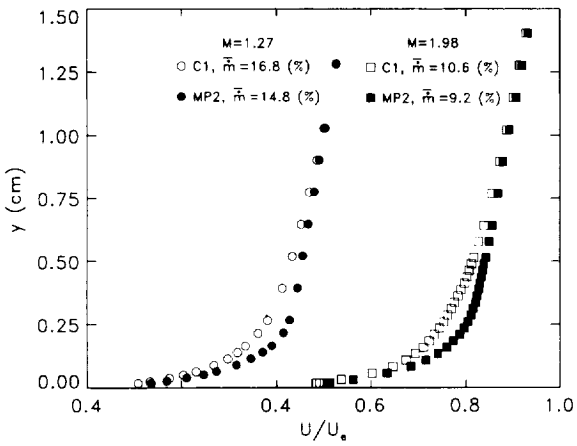

Fig. 13 Near-wall normalized velocity profiles, C1 and MP2 plates.

Concluding Remarks

An experimental program has been conducted to study honeycomb composite materials as possible boundary-layer bleed materials. The results of the study may be summarized as follows.

1. Using the normal hole perforated solid plate as a reference, the two porous honeycomb plates were significantly less efficient at removing boundary-layer mass. The plate with four holes per cell performed slightly better than the plate with one hole per cell.
2. The 31% and 21% porosity microporous plates flowed about the same as the baseline perforated solid plate. The exception being the 31% porosity plate at near-choke conditions where the flow coefficient was slightly less than the baseline distribution.
3. The 9% porosity microporous plate was surprisingly more efficient than the baseline plate. The reasons for this are unclear at present.
4. The microporous skins were more effective at reducing the incompressible shape factor than the porous honeycomb or baseline configurations. For the undistorted approach boundary-layer, bleeding beyond 25% of the approach boundary-layer mass flow yielded no further reduction.

Future work relating to the honeycomb composites will be focused on several areas which include:

1. Evaluation of the microporous honeycomb in a more production type configuration.
2. Evaluation of microporous honeycomb with streamwise slots and angled honeycomb intended to improve pressure recovery across the bleed band by simulating angled bleed orifices.
3. Evaluation of all configurations with a distorted approach boundary-layer.

Acknowledgments

The authors would like to acknowledge C. Parente of Northrop Grumman for providing the microporous skin and backing honeycomb and J. Koncsek of the Boeing Company for providing the nacelle honeycomb material.

References

[1] Dennard, J. S., "A Transonic Investigation of the Mass-Flow and Pressure Recovery Characteristics of Several Types of Auxiliary Air Inlets," NACA Research Memorandum RM L57B07, Apr. 1957.

[2] McLafferty, G. M. and Ranard, E., "Pressure Losses and Flow Coefficients of Slanted Perforations Discharging from Within a Simulated Supersonic Inlet," United Aircraft Corporation Report R-0920-1, Dec. 1958.

[3] Willis, B. P., Davis, D. O., and Hingst, W. R., "Flow Coefficient Behavior for Boundary-Layer Bleed Holes and Slots," AIAA Paper 95-0031, Jan. 1995.

[4] Willis, B. P., Davis, D. O., and Hingst, W. R., "Flowfield Measurements in a Normal-Hole-Bled Oblique Shock-Wave and Turbulent Boundary-Layer Interaction," AIAA Paper 95-2885, July 1995.

[5] Willis, B. P. and Davis, D. O., "Boundary-Layer Development Downstream of a Bleed Mass Flow Removal Region," AIAA Paper 96-3278, July 1996.

[6] Chyu, W. J., Rimlinger, M. J., and Shih, T. I.-P., "Effects of Bleed-Hole Geometry and Plenum Pressure on Three-Dimensional Shock-Wave/Boundary-Layer/Bleed Interactions," AIAA Paper 93-3259, July 1993.

[7] Davis, D. O., Willis, B. P., and Hingst, W. R., "Flowfield Measurements Inside a Boundary-Layer Bleed Slot," *AIAA Journal*, Vol. 34, Oct. 1996, pp. 1977–1983.

[8] Syberg, J. and Hickcox, T. E., "Design of a Bleed System for a Mach 3.5 Inlet," NASA Contractor Report 2187, Jan. 1973.

[9] Davis, D. O., Willis, B. P., Hunter, G. W., Liu, C.-C., and Wu, Q., "Mass Flow Measurement Using a Hydrocarbon Trace-Gas Technique," *Proceedings of the Fluids Engineering Division Summer Meeting*, Vol. 4, FED-Vol. 239, ASME, 1996, pp. 465–469.

[10] Blumenthal, P. Z., "A PC Program for Estimating Measurement Uncertainty for Aeronautics Test Instrumentation," AIAA Paper 95-3072, July 1995.

[11] Davis, D. O., Grimes, M., and Schoenenberger, M., "Effect of Flow Misalignment and Multi-Hole Interaction on Boundary-Layer Bleed Hole Flow Coefficient Behavior," *Prepared for the 1996 International Mechanical Engineering Congress and Exhibit*, ASME, Nov. 17-24, 1996.

REPORT DOCUMENTATION PAGE

Form Approved
OMB No. 0704-0188

1. AGENCY USE ONLY (*Leave blank*)	2. REPORT DATE	3. REPORT TYPE AND DATES COVERED
	September 1997	Technical Memorandum

4. TITLE AND SUBTITLE

Porous and Microporous Honeycomb Composites as Potential Boundary-Layer Bleed Materials

5. FUNDING NUMBERS

WU-523-36-13-00

6. AUTHOR(S)

D.O. Davis, B.P. Willis, and M. Schoenenberger

7. PERFORMING ORGANIZATION NAME(S) AND ADDRESS(ES)

National Aeronautics and Space Administration
Lewis Research Center
Cleveland, Ohio 44135-3191

8. PERFORMING ORGANIZATION REPORT NUMBER

E-10911

9. SPONSORING/MONITORING AGENCY NAME(S) AND ADDRESS(ES)

National Aeronautics and Space Administration
Washington, DC 20546-0001

10. SPONSORING/MONITORING AGENCY REPORT NUMBER

NASA TM-113160
AIAA-97-3260

11. SUPPLEMENTARY NOTES

Prepared for the 33rd Joint Propulsion Conference and Exhibit cosponsored by AIAA, ASME, SAE and ASEE, Seattle, Washington, July 6-9, 1997. D.O. Davis and B.P. Willis, NASA Lewis Research Center; M. Schoenenberger, Case Western Reserve University, Cleveland, Ohio. Responsible person, D.O. Davis, organization code 5850, (216) 433-8116.

12a. DISTRIBUTION/AVAILABILITY STATEMENT

Unclassified - Unlimited
Subject Categories 07 and 34

This publication is available from the NASA Center for AeroSpace Information, (301) 621-0390.

12b. DISTRIBUTION CODE

13. ABSTRACT (*Maximum 200 words*)

Results of an experimental investigation are presented in which the use of porous and microporous honeycomb composite materials is evaluated as an alternate to perforated solid plates for boundary-layer bleed in supersonic aircraft inlets. The terms "porous" and "microporous," respectively, refer to bleed orifice diameters roughly equal to and much less than the displacement thickness of the approach boundary-layer. A Baseline porous solid plate, two porous honeycomb, and three microporous honey comb configurations are evaluated. The performance of the plates is characterized by the flow coefficient and relative change in boundary-layer profile parameters across the bleed region. The tests were conducted at Mach numbers of 1.27 and 1.98. The results show the porous honeycomb is not as efficient at removing mass compared to the baseline. The microporous plates were about equal to the baseline with one plate demonstrating a significantly higher efficiency. The microporous plates produced significantly fuller boundary-layer profiles downstream of the bleed region for a given mass flow removal rate than either the baseline or the porous honeycomb plates.

14. SUBJECT TERMS	15. NUMBER OF PAGES
Supersonic flow; Boundary layer control	13
	16. PRICE CODE: A03

17. SECURITY CLASSIFICATION OF REPORT	18. SECURITY CLASSIFICATION OF THIS PAGE	19. SECURITY CLASSIFICATION OF ABSTRACT	20. LIMITATION OF ABSTRACT
Unclassified	Unclassified	Unclassified	